Directed flow indicates a cross-over deconfinement transition in relativistic nuclear collisions

Yu. B. Ivanov[1,2,*] and A. A. Soldatov[2,†]
[1]*National Research Centre (NRC) "Kurchatov Institute," 123182 Moscow, Russia*
[2]*National Research Nuclear University "MEPhI" (Moscow Engineering Physics Institute), 115409 Moscow, Russia*
(Received 9 December 2014; published 26 February 2015)

Analysis of directed flow (v_1) of protons, antiprotons, and pions in heavy-ion collisions is performed in the range of incident energies $\sqrt{s_{NN}} = 2.7$–27 GeV. Simulations have been done within a three-fluid model employing a purely hadronic equation of state (EoS) and two versions of the EoS involving deconfinement transitions: a first-order phase transition and a smooth crossover transition. High sensitivity of the directed flow, especially the proton one, to the EoS is found. The crossover EoS is favored by the most part of considered experimental data. A strong wiggle in the excitation function of the proton v_1 slope at the midrapidity obtained with the first-order-phase-transition EoS and a smooth proton v_1 with positive midrapidity slope, within the hadronic EoS unambiguously disagree with the data. The pion and antiproton v_1 also definitely testify in favor of the crossover EoS. The results obtained with deconfinement EoS's apparently indicate that these EoS's in the quark-gluon sector should be stiffer at high baryon densities than those used in the calculation.

DOI: 10.1103/PhysRevC.91.024915 PACS number(s): 25.75.Nq, 25.75.Ld, 24.10.Nz

I. INTRODUCTION

The directed flow [1] of particles has been one of the key observables, since the first data on the heavy-ion collisions became available at the Bevalac. Nowadays it is defined as the first coefficient, v_1, in the Fourier expansion of a particle distribution, $d^2N/dy\,d\phi$, in azimuthal angle ϕ with respect to the reaction plane [2,3]

$$\frac{d^2N}{dy\,d\phi} = \frac{dN}{dy}\left(1 + \sum_{n=1}^{\infty} 2\,v_n(y)\cos(n\phi)\right), \qquad (1)$$

where y is a longitudinal rapidity of a particle. The directed flow is mainly formed at an early (compression) stage of the collisions and hence is sensitive to early pressure gradients in the evolving nuclear matter [4,5]. As the EoS is harder, stronger pressure is developed. Thus the flow reflects the stiffness of the nuclear EoS at the early stage of nuclear collisions [6,7], which is of prime interest for heavy-ion research. A retrospective review and a survey of developments in the field of the collective flow are presented in a recent article [8].

Directed flow has been extensively exploited to obtain information on the EoS. In particular, it was predicted that the first-order transition to the quark-gluon phase (QGP) results in significant reduction of the directed flow [9–11] (the so-called "softest-point" effect), because the pressure gradients in the mixed phase are lower than those in pure hadronic and quark-gluon phases. The v_1 data [12,13] from the BNL Alternating Gradient Synchrontron (AGS) indeed demonstrate a graduate fall of the slope of $v_1(y)$ at midrapidity with the incident energy rise from $\sqrt{s_{NN}} = 2.7$ GeV ($E_{\rm lab} = 2\ A\cdot$GeV) to 4.3 GeV ($E_{\rm lab} = 8\ A\cdot$GeV). This finding was further developed within fluid-dynamical models [14,15]. It was found that the directed flow as a function of rapidity exhibits a wiggle near the midrapidity with a negative slope near the midrapidity, when the incident energy is in the range corresponding to onset of the first-order phase transition. This occurs because the event shape at these energies resembles an ellipsoid in coordinate space, tilted with respect to the beam axis. This ellipsoid expands predominantly orthogonal to its short dimension, forming a so-called "third component" [14] or "antiflow" [15] near the midrapidity. When the softest point is passed, i.e., the incident energy is above that corresponding to the onset of the first-order phase transition, the midrapidity v_1 slope reaches a maximum. After that the v_1 slope decreases again [10,11,15,16]. Thus, the wiggle near the midrapidity and the wiggle-like behavior of the excitation function of the midrapidity v_1 slope were put forward as a signature of the QGP phase transition. Measurements of the directed flow by the NA49 Collaboration [17] at the CERN Super Proton Synchrotron (SPS) had insufficient statistics to draw definite conclusions on the presence or absence of such a v_1 wiggle at the midrapidity.

However, the midrapidity v_1 wiggle can have a different physical origin. The QGP EoS is not a necessarily prerequisite to reach the stopping needed to create this tilted source [18]. A combination of space-momentum correlations—characteristic of radial expansion together with the correlation between the position of a nucleon in the fireball and its stopping—may result in a negative slope in the rapidity dependence of the directed flow in high-energy nucleus-nucleus collisions.

The elliptic flow, v_2, and the triangular flow, v_3, have been extensively studied both theoretically and experimentally in recent years by about five orders of magnitude in the collision energy $\sqrt{s_{NN}}$ [19]. In contrast, apart from these early measurements and until recently, the directed flow was insufficiently experimentally studied to check the above predictions. The interest in the directed flow has recently been revived due to data obtained by the STAR Collaboration within the framework of the beam energy scan (BES) program at the BNL Relativistic Heavy Ion Collider (RHIC) [20]. The directed flow of identified hadrons—protons, antiprotons, and positive and negative pions—has been measured with high

*Y.Ivanov@gsi.de
†saa@ru.net

precision for Au+Au collisions in the energy range $\sqrt{s_{NN}} =$ (7.7–39) GeV. These data, together with earlier experimental results from the AGS [12,13] and SPS [17], provide a basis for theoretical analysis of the directed flow in a wide energy range.

These data have been already addressed in Refs. [21,22]. The Frankfurt group [21] confined itself to incident energies $\sqrt{s_{NN}} < 20$ GeV. However, the authors of Ref. [21] did not describe the data and obtain conclusive results. In a hybrid approach [23], the authors found that there is no sensitivity of the directed flow on the EoS and, in particular, on the existence of a first-order phase transition. The reason for this result could be that the initial interpenetration stage of the collision is described within the ultrarelativistic quantum molecular dynamics (UrQMD) [24] for all scenarios (with and without transition to the QGP) in the hybrid approach [23]. Because of the UrQMD model, the effective EoS during this stage is purely hadronic. Only later, when transition from initial UrQMD transport to the fluid dynamics happens, different scenarios start to differ. As mentioned above, the directed flow is mainly formed at the early stage of the collisions [4,5]. Therefore, in all scenarios considered in the hybrid approach [23], the directed flow was mainly formed at the purely hadronic UrQMD stage, thus exhibiting similar results for different scenarios.

In Ref. [22] the STAR data were analyzed within two complementary approaches: kinetic transport approaches of the parton-hadron string dynamics (PHSD) [25] and the hadron string dynamics (HSD) [26]) and a hydrodynamic approach of the relativistic three-fluid dynamics (3FD) [27,28]. The PHSD model includes a crossover-type transition into the QGP, while the HSD one is a purely hadronic version of the PHSD. The 3FD simulations were performed with two EoS's: a purely hadronic EoS [29] and a EoS with a crossover transition into the QGP [30]. It was found that the directed flow is sensitive to the EoS. The crossover scenario within both the PHSD and 3FD provides the best (but not perfect) results, being in reasonable agreement with the STAR data.

In the present paper we extend the analysis performed in Ref. [22] within the 3FD model. Results for a EoS with a first-order phase transition [30] are reported. The AGS [13] and SPS [17] data are considered in detail on equal footing with the STAR results. Computations are performed with somewhat higher accuracy, i.e., a finer grid and larger numbers of test particles,[1] than that even in Ref. [22]. In contrast to other observables, the directed flow is very sensitive to the accuracy settings of the numerical scheme. Accurate calculations require very high memory and computation time. In particular, due to this reason we failed to perform calculations for energies above $\sqrt{s_{NN}} = 30$ GeV. Note that the change of other observables analyzed so far [28,31–36], due to higher accuracy, is below 15% as compared to results of previous calculations.

II. THE 3FD MODEL

The 3FD model [27] is an extension of a two-fluid model with radiation of direct pions [37–39] and a (2+1)-fluid model [40,41]. These models have been further elaborated to include a baryon-free (the so-called fireball) fluid on an equal footing with the baryon-rich ones. A certain formation time was introduced for the fireball fluid, during which the matter of the fluid propagates without interactions. The formation time is associated with a finite time of string formation and decay and is incorporated also in the kinetic transport models such as PHSD/HSD [25,26] and UrQMD [24].

The 3FD model [27] describes a nuclear collision from the stage of the incident cold nuclei approaching each other, to the final freeze-out stage. Contrary to the conventional one-fluid dynamics, where a local instantaneous stopping of matter of the colliding nuclei is assumed, the 3FD considers an interpenetrating counterstreaming flows of leading baryon-rich matter, which gradually decelerate each other due to mutual friction. The basic idea of a 3FD approximation to heavy-ion collisions [42,43] is that a generally nonequilibrium distribution of baryon-rich matter at each space-time point can be represented as a sum of two distinct contributions initially associated with constituent nucleons of the projectile and target nuclei. In addition, newly produced particles, populating predominantly the midrapidity region, are associated with the fireball fluid. Therefore, the 3FD approximation is a minimal way to simulate the early-stage nonequilibrium state of the colliding nuclei at high incident energies.

Friction forces between fluids are the key ingredients of the model that determine dynamics of the nuclear collision. The friction forces in the hadronic phase were estimated in Ref. [44] based on experimental inclusive proton-proton cross sections. In order to reproduce the baryon stopping at high incident energies, this estimated friction between counterstreaming fluids was enhanced within the hadronic scenario [28]. Though such enhancement is admissible in view of uncertainties of the estimated friction, the value of the enhancement looks too high. In deconfinement scenarios there is no need to modify the hadronic friction [28]. This can be considered as an indirect argument in favor of such scenarios. At the same time, the friction forces in the QGP are purely phenomenological. They were fitted to reproduce the baryon stopping at high incident energies within the deconfinement scenarios. There are no theoretical estimates of the QGP friction in terms of the QGP dynamics so far. A parton cascade model [45] offers a possible ground for such estimate. This approach predicts a fast kinetic equilibration (on a scale of 1 fm/c), mainly driven by the inelastic processes. Therefore, a reasonably strong QGP friction can be anticipated in this approach. Another promising way for such estimate can be based on an effective string rope model [46,47]. Proceeding from coherent Yang-Mills field theoretical approach, this model introduces an effective string tension based on Monte Carlo string cascade and parton cascade model results. The effective string tension causes substantial baryon stopping in heavy-ion collisions.

[1] A numerical "particle-in-cell" scheme is used in the present simulations; see Ref. [27] and references therein for more details. The matter transfer due to pressure gradients and friction between fluids is computed on a fixed grid (the so-called Euler step of the scheme). An ensemble of Lagrangian test particles is used for the calculation of the drift transfer of the baryonic charge, energy, and momentum (the so-called Lagrangian step of the scheme).

In particular, for semicentral collisions, this model predicts formation of a compact initial QGP fireball in the form of a tilted disk. Thus, it naturally explains the origin of the above-discussed "antiflow" or "third flow component."

Different EoS's can be implemented in the 3FD model. All three fluids are described by the same EoS (chosen for the simulation), of course, with their specific values of the thermodynamic quantities. At the initial stage of the reaction all three fluids coexist in the same space-time region, thus describing a certain *nonequilibrium* state of the matter. It may happen that one or two of the fluids occur in the quark-gluon phase while other(s) is (are) in the hadronic one. This is a kind of a nonequilibrium mixed phase that is also possible in the model. A key point is that the 3FD model is able to treat a deconfinement transition at the early *nonequilibrium* stage of the collision, when the directed flow is mainly formed, as was mentioned above. This makes 3FD predictions for v_1, at least, sensitive to the used EoS.

In this work we apply a purely hadronic EoS [29], an EoS with a crossover transition as constructed in Ref. [30], and an EoS with a first-order phase transition into the QGP [30]. In recent works [28,31–36] an analysis of the major part of bulk observables has been performed with these three EoS's: the baryon stopping [28,34], yields of different hadrons, their rapidity and transverse momentum distributions [31,32], as well as the elliptic flow excitation function [35,36]. Comparison with available data, including those at RHIC energies, indicated a definite advantage of the deconfinement (crossover and first-order) scenarios over the purely hadronic one, especially at high collision energies. However, predictions of the crossover and first-order-transition scenarios looked very similar so far. Only a slight preference could be given to the crossover EoS, though the latter does not perfectly reproduced the data either. The physical input of the present 3FD calculations is described in detail in Ref. [28]. No tuning (or change) of physical 3FD-model parameters has been done in the present study as compared to that stated in Ref. [28]. A more detailed discussion of the features of the 3FD model can be found in Refs. [27,28,36].

III. DIRECTED FLOW WITHIN ALTERNATIVE SCENARIOS

As mentioned above, calculations of the directed flow require a high numerical accuracy, i.e., a fine computational grid and a large number of test particles. This high accuracy is needed to accurately describe the initial stage of the collision, where pressure gradients in the evolving nuclear matter are high. The accuracy at this stage is decisive for the directed flow because the latter is mainly formed at the early nonequilibrium stage of the collisions. The accuracy requirements result in high computation memory consumption that rapidly increases with the collision energy, approximately as $\propto s_{NN}$, and a long computation time, $\propto (s_{NN})^{3/2}$. The reason of this rapid rise is the Lorentz contraction of incident nuclei, as described in Ref. [27] in detail. On the one hand, the grid in the beam, Lorentz-contracted direction, should be fine enough for a reasonable description of the longitudinal gradients of the matter. From the practical point of view, it is desirable to have 60 cells on the Lorentz-contracted nuclear diameter.[2] On the other hand, to minimize a numerical diffusion in the computational scheme, an equal-step grid in all directions ($\Delta x : \Delta y : \Delta z = 1 : 1 : 1$) should be taken, in spite of Lorentz contraction of incident nuclei, which is quite strong at high energies. This choice makes the scheme isotropic with respect to the numerical diffusion. However, it makes the grid too fine in the transverse directions and thus results in high memory consumption. The need for the equal-step grid in all directions for relativistic hydrodynamic computations within a conventional one-fluid model was pointed out in Ref. [48]. As it was demonstrated there, the matter transport becomes even acausal if this condition is strongly violated.

In the simulations the acceptance $p_T < 2$ GeV/c for transverse momentum (p_T) of the produced particles is applied to all hadrons at all considered incident energies. In the 3FD model, particles are not isotopically distinguished; i.e., the model deals with nucleons, pions, etc., rather than with protons, neutrons, π^+, π^-, and π^0. Therefore, the v_1 values of protons, antiprotons, and pions presented below, in fact, are v_1 of nucleons, antinucleons, and all (i.e. π^+, π^-, and π^0) pions. Simulations are performed for midcentral collisions: impact parameter $b = 6$ fm for Au+Au collisions and $b = 6.5$ fm for Pb + Pb collisions.

The directed flow $v_1(y)$ as a function of rapidity y at BES-RHIC bombarding energies is presented in Fig. 1 for pions, protons, and antiprotons. As seen, the 3FD model does not perfectly describe the $v_1(y)$ distributions. However, we can definitely conclude that the best overall reproduction of the STAR data is achieved with the crossover EoS. The first-order transition scenario gives results which strongly differ from those in the crossover scenario, especially for the proton v_1. This is in contrast to other bulk observable analyzed so far [28,31–36].

At $\sqrt{s_{NN}} \leqslant 20$ GeV the the crossover EoS is certainly the best in reproduction of the proton $v_1(y)$. However, surprisingly the hadronic scenario becomes preferable for the proton $v_1(y)$ at $\sqrt{s_{NN}} > 20$ GeV. A similar situation takes place in the PHSD-HSD transport approach. Indeed, predictions of the HSD model (i.e., without a deconfinement transition) for the proton $v_1(y)$ become preferable at $\sqrt{s_{NN}} > 30$ GeV [22], i.e., at somewhat higher energies than in the 3FD model. However, the difference between the PHSD and HSD results for protons is small at these energies. Moreover, the proton v_1 predicted by the UrQMD model, as cited in the experimental paper [20] and in the recent theoretical work [21], better reproduces the proton $v_1(y)$ data at high collision energies than the PHSD and 3FD-deconfinement models do. Note that the UrQMD model is based on the hadronic dynamics. All these observations could be considered as an evidence of a problem in the QGP sector of a EoS. However the pion and antiproton v_1 contradict such a conclusion. Indeed, the pion and antiproton directed flow definitely indicates a preference

[2]However, only 40 cells per the Lorentz-contracted nuclear diameter were possible to implement at $\sqrt{s_{NN}} > 10$ GeV in order to confine the required memory and thus to complete the computation in a reasonable time.

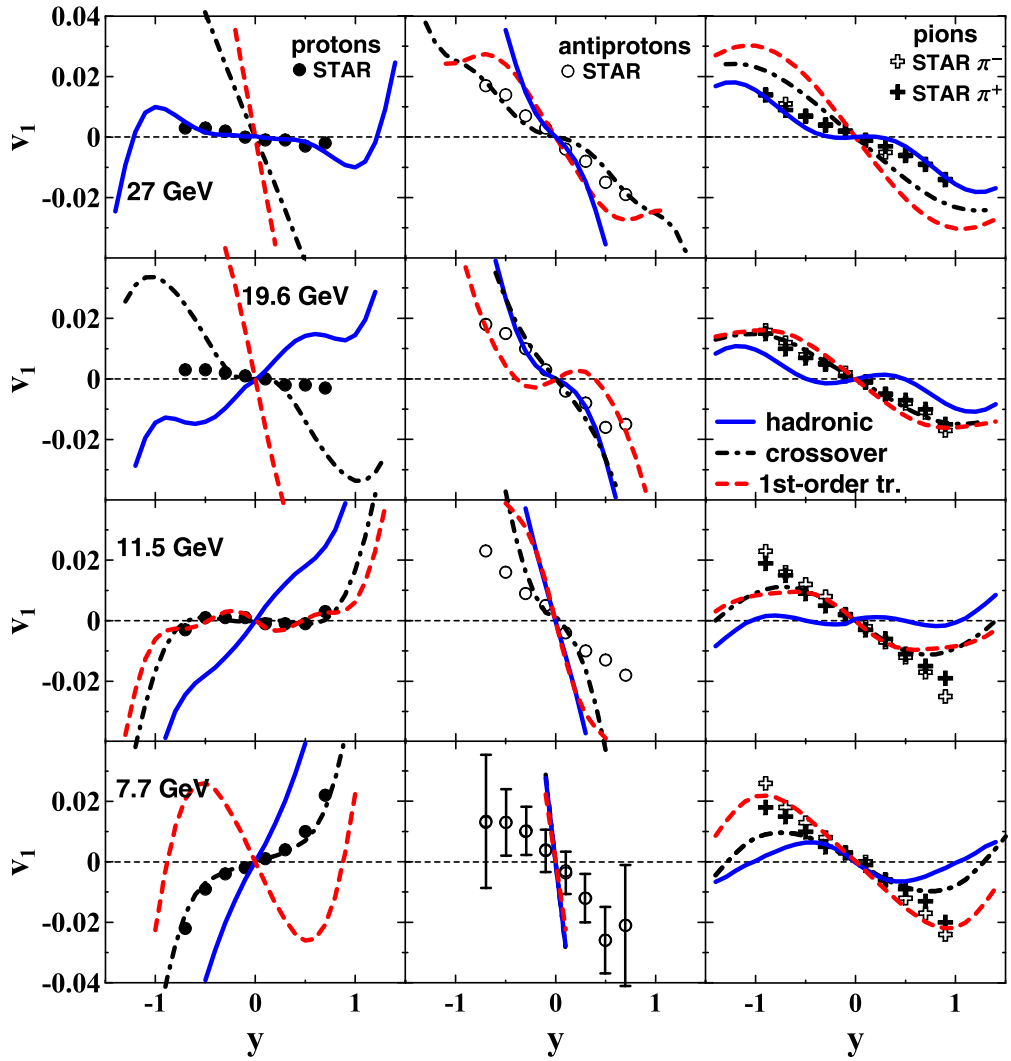

FIG. 1. (Color online) The directed flow $v_1(y)$ for protons, antiprotons, and pions from midcentral ($b = 6$ fm) Au+Au collisions at various collision energies from $\sqrt{s_{NN}} = 7.7$ to 27 GeV calculated with different EoS's. Experimental data are from the STAR Collaboration [20].

of the crossover scenario at the same collision energies within both the PHSD-HSD and 3FD approaches.

This puzzle has a natural resolution within the 3FD model. The the QGP sector of the EoS's with deconfinement [30] was fitted to the lattice QCD data at zero net-baryon density and just extrapolated to nonzero baryon densities. The protons mainly originate from baryon-rich fluids that are governed by the EoS at finite baryon densities. The too-strong antiflow at $\sqrt{s_{NN}} = 27$ GeV may be a sign of too-soft QGP EoS. Note that a weak flow or antiflow indicates softness of a EoS. Predictions of the first-order-transition EoS, the QGP sector of which is constructed in the same way as that of the crossover one, fail even at lower collision energies, when the QGP starts to dominate in the collision dynamics, i.e., at $\sqrt{s_{NN}} \gtrsim 15$ GeV. This fact indirectly supports the conjecture on a too-soft QGP sector at high baryon densities in the used EoS's. At the same time, the baryon-free (fireball) fluid is governed by the EoS at zero net-baryon density. This fluid is a main source of antiprotons (∼80% near midrapidity at $\sqrt{s_{NN}} = 27$ GeV and $b = 6$ fm), the directed flow of which is in good agreement with the data at $\sqrt{s_{NN}} = 27$ GeV within the crossover scenario and in reasonable agreement even within the first-order-transition scenario. It is encouraging because at zero net-baryon density the QGP sector of the EoS's is fitted to the lattice QCD data. The pions are produced from all fluids: near midrapidity ∼50% from the baryon-rich fluids and ∼50% from the baryon-free one at $\sqrt{s_{NN}} = 27$ GeV. Hence, the disagreement of the pion v_1 with data is quite moderate at $\sqrt{s_{NN}} = 27$ GeV.

As seen from Fig. 1, the deconfinement scenarios are definitely preferable for the pion $v_1(y)$. The pion data at 7.7 GeV are slightly better reproduced within the first-order-transition scenario, while at 27 GeV the crossover scenario is preferable. The antiproton $v_1(y)$ data testify in favor of the crossover scenario, except for the energy of 7.7 GeV, where all scenarios equally fail. It should be taken into account that the antiproton multiplicity in the midcentral ($b = 6$ fm) Au+Au collision at 7.7 Gev is 1 within the deconfinement scenarios and 3 within the hadronic scenario. Therefore, the hydrodynamical approach based on the grand canonical ensemble is definitely inapplicable to the antiprotons in this case.

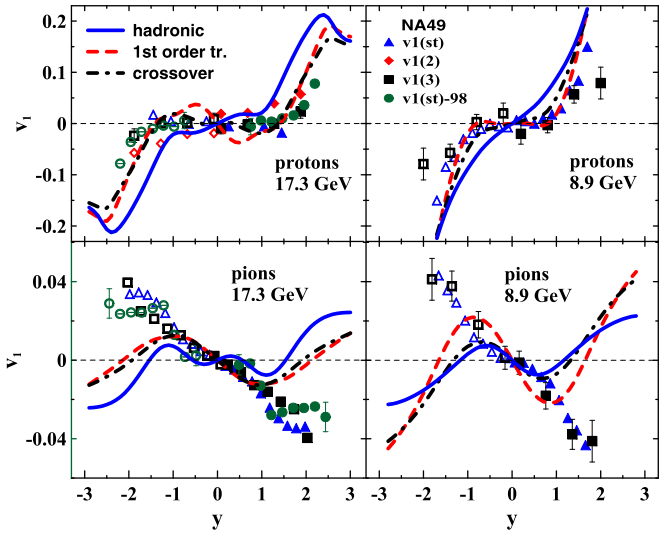

FIG. 2. (Color online) The directed flow $v_1(y)$ for protons and pions from midcentral ($b = 6.5$ fm) Pb + Pb collisions at collision energies $\sqrt{s_{NN}} = 8.9$ and 17.3 GeV calculated with different EoS's. Experimental data of the NA49 Collaboration [17] obtained by two different methods are displayed: the standard method [v(st)] and the method of n-particle correlations [v(n)]. Solid symbols correspond to measured data, while open symbols are those reflected with respect to the midrapidity. Updated data of the NA49 Collaboration [49] [v(st)-98] are also shown.

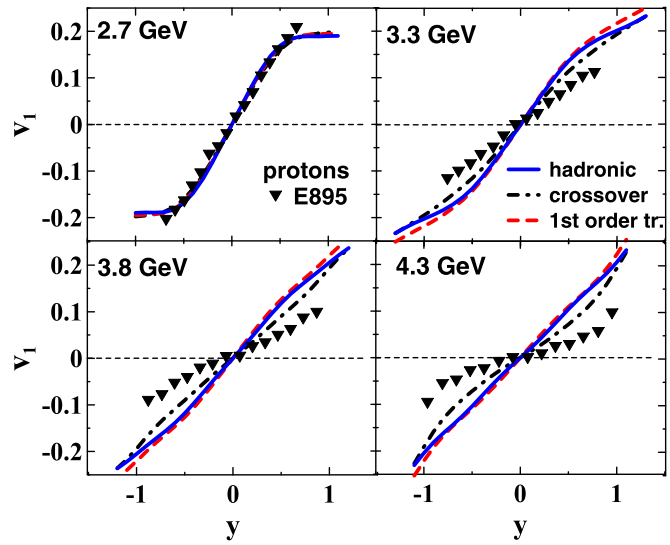

FIG. 3. (Color online) The directed flow $v_1(y)$ for protons from midcentral ($b = 6$ fm) Au+Au collisions at various collision energies from $\sqrt{s_{NN}} = 2.7$ to 4.3 GeV calculated with different EoS's. Experimental data are from the E895 Collaboration [13].

Figure 2 displays a comparison of the calculated proton and pion directed flow from midcentral Pb + Pb collisions with the NA49 data [17] obtained at the SPS. The comparison definitely testify in favor of the deconfinement scenarios, though it is difficult to choose between the first-order-transition and crossover scenarios. While the deconfinement scenarios give a reasonable agreement with the proton $v_1(y)$ in the whole range of rapidities, the pion $v_1(y)$ is well reproduced only in the midrapidity region. The calculated pion $v_1(y)$ manifests a wiggle in the midrapidity region while the data are monotonous functions of y. A similar situation takes place at two lower collision energies in Fig. 1. A probable reason for this poor reproduction of the pion v_1 at peripheral rapidities is that the hydrodynamic freeze-out disregards shadowing of a part of the frozen-out particles by still hydrodynamically evolving matter. This mechanism was discussed in Refs. [7,50]. The shadowing means that frozen-out particles cannot freely propagate through the region still occupied by the hydrodynamically evolving matter but rather become reabsorbed into the hydrodynamic phase. This shadowing is especially effective at the peripheral rapidities, where slowly evolving near-spectator baryon-rich blobs prevent pions with $p_x > 0$ at $y > 0$ and $p_x < 0$ at $y < 0$ from escaping (here p_x is the transverse momentum in the reaction plane).[3] This makes the pion v_1 slope opposite in sign to the proton v_1 slope at the peripheral rapidities. The hydrodynamic freeze-out does not take into account this shadowing, and hence, the hydrodynamic pion and proton v_1 slopes at the peripheral rapidities are of the same sign.

The directed flow $v_1(y)$ for protons from midcentral Au+Au collisions at various collision energies from $\sqrt{s_{NN}} = 2.7$ to 4.3 GeV ($E_{\rm lab} = 2$, 4, 6, and 8 $A \cdot$ GeV) calculated with different EoS's and its comparison with experimental data from the E895 Collaboration [13] are presented in Fig. 3. As seen, at $\sqrt{s_{NN}} = 2.7$ GeV predictions of all EoS's are identical (as it is expected) and are in good agreement with the data. With the collision energy rise the predictions of different EoS's start to differ. First, the crossover $v_1(y)$ decouples from two others because the QGP fraction starts from very low densities in the crossover EoS while the first-order phase transition in the corresponding EoS is not reached yet. At the same time, the agreement with the data worsens with the collision energy rise. The QGP fraction moves the crossover $v_1(y)$ closer to the data, though insufficiently close.

The E895 Collaboration also presented the data [13] in terms of the conventional transverse-momentum flow defined as [1]

$$\langle P_x \rangle(y) = \frac{\int d^2 p_T \; p_x \; E \; dN/d^3 p}{\int d^2 p_T \; E \; dN/d^3 p}, \qquad (2)$$

where p_x is the transverse momentum of in the reaction plane, $E\,dN/d^3p$ is the invariant momentum distribution of a particle with E being the particle energy, and integration runs over the transverse momentum p_T. These data together with results of the 3FD simulations are presented in Fig. 4. It is surprising that agreement of the $\langle P_x \rangle(y)$ calculated within all scenarios is much better than that in terms of $v_1(y)$. The crossover $\langle P_x \rangle(y)$ almost perfectly reproduces the data at all AGS energies. Transverse-momentum spectra of protons, which are required for recalculations of $\langle P_x \rangle(y)$ into $v_1(y)$, are reasonably well

[3] Conventionally, it is assumed that the projectile spectator is situated at positive x and moves with positive rapidity, while the target spectator, at negative x and moves with negative rapidity.

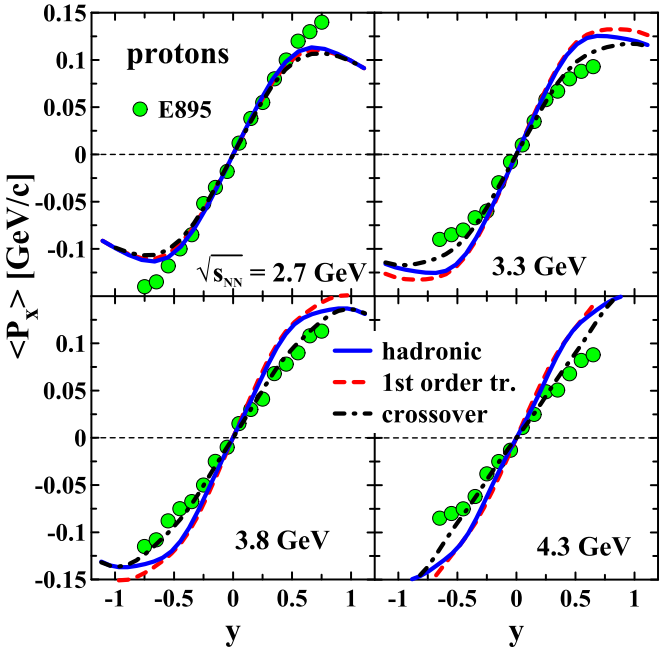

FIG. 4. (Color online) The same as in Fig. 3 but in terms of the transverse flow $\langle P_x \rangle(y)$.

reproduced within all scenarios in the considered energy range [32,51]. Figure 5 illustrates the reproduction of inverse-slope parameters of transverse-mass spectra of protons, which are the only quantities that are relevant to calculations of $v_1(y)$ and $\langle P_x \rangle(y)$. These inverse slopes T were deduced from fitting both the experimental [52] and calculated proton spectra by the formula

$$\frac{d^2N}{m_T\, dm_T\, dy} \propto m_T \exp\left(-\frac{m_T}{T}\right), \tag{3}$$

where $m_T = \sqrt{m^2 + p_T^2}$ and y are the transverse mass and rapidity, respectively. Figure 5 presents the calculated inverse-slope parameters of protons produced in Au+Au collisions at incident energies $\sqrt{s_{NN}} = 3.8$ and 4.3 GeV at various centralities as a function of rapidity and their comparison with the experimental data of the E917 Collaboration [52]. As seen, the agreement with the data is indeed good, especially for the crossover EoS. In view of this agreement with the data on the transverse-mass spectra, it is puzzling that the degrees of reproduction of the $\langle P_x \rangle(y)$ and $v_1(y)$ data are so different.

IV. MIDRAPIDITY SLOPE OF DIRECTED FLOW

The slope of the directed flow at the midrapidity is often used to quantify variation of the directed flow with collision energy. The excitation functions for the slopes of the v_1 distributions at midrapidity are presented in Fig. 6. As noted above, the best reproduction of the data is achieved with the crossover EoS. The proton dv_1/dy within the first-order-transition scenario exhibits a wiggle earlier predicted in Refs. [10,11,15,16]. In the present case the wiggle is mostly located in the negative range of slopes. The first-order-transition results demonstrate the worst agreement with

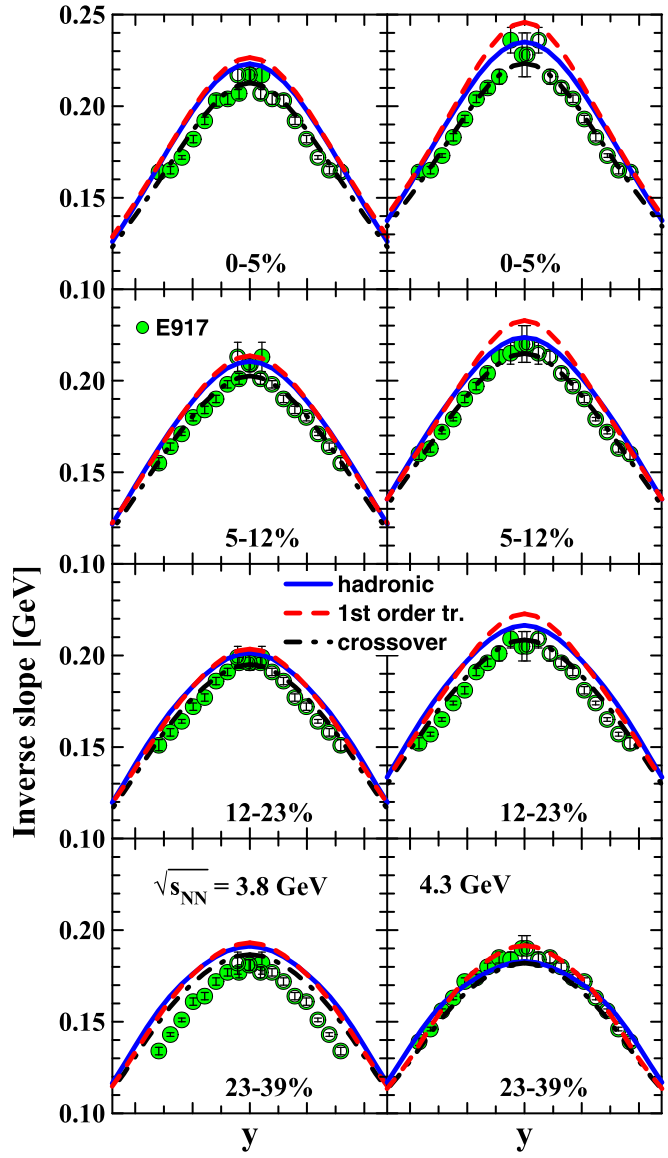

FIG. 5. (Color online) Inverse-slope parameter of transverse-mass spectra of protons, cf. T in Eq. (3), produced in Au+Au collisions at incident energies $\sqrt{s_{NN}} = 3.8$ GeV (left column) and 4.3 GeV (right column) [$E_{\rm lab} = 6A$ and $8A$ GeV] at various centralities as a function of rapidity. The percentage indicates the centrality, i.e., the fraction of the total reaction cross section, corresponding to experimental selection of events. The 3FD results are presented for impact parameters $b = 2$, 4, 6, and 8 fm (from top row of panels to bottom one). Experimental data are from E917 Collaboration [52]. Solid symbols correspond to measured data, while open symbols are those reflected with respect to the midrapidity.

the proton and antiproton data on dv_1/dy. The discrepancies between experiment and the 3FD predictions are smaller for the purely hadronic EoS; however, the agreement with the 3FD model for the crossover EoS is definitely better, though it is far from being perfect. All the above discussed problems of the crossover scenario at low and high collision energies reveal themselves in the dv_1/dy plot.

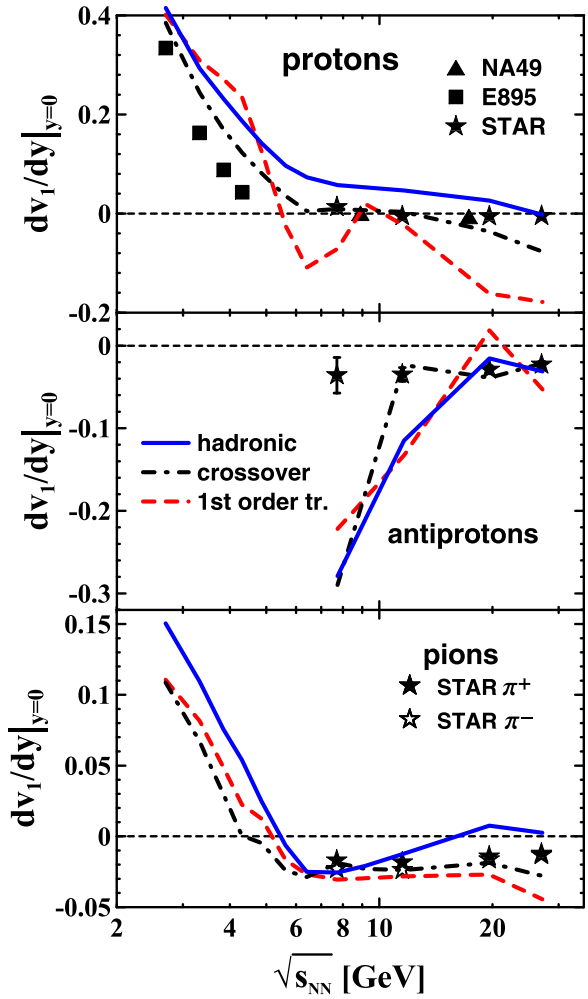

FIG. 6. (Color online) The beam energy dependence of the directed flow slope at midrapidity for protons, antiprotons, and pions from midcentral ($b = 6$ fm) Au+Au collisions calculated with different EoS's. The experimental data are from the STAR measurements [20] and prior experiments with comparable acceptance cuts [13,17].

The crossover scenario well reproduces the pion slopes at all measured energies and the antiproton slopes at $\sqrt{s_{NN}} > 10$ GeV. Note that the 3FD model is poorly applicable to description of antiprotons at $\sqrt{s_{NN}} < 10$ GeV in view of a low antiproton multiplicity. In the case of proton slopes the crossover scenario fails both at low ($\sqrt{s_{NN}} < 5$ GeV) and high ($\sqrt{s_{NN}} > 20$ GeV) collision energies. The failure at low energies is still questionable because the same data but in terms of $\langle P_x \rangle$ are almost perfectly reproduced by the crossover scenario; see Fig. 4. As for the highest computed energy of $\sqrt{s_{NN}} = 27$ GeV, this simulation has been performed at the edge of computational abilities of the code. Therefore, the disagreement with the data could be, at least partially, because the 27-GeV results still suffer from insufficient accuracy. In the present paper the accuracy of the 27-GeV computation is slightly higher that in Ref. [22]: 40 cells per the Lorentz-contracted nuclear diameter instead of 35 in Ref. [22]. This made the calculated dv_1/dy slightly closer to the experimental value: -0.077 instead of -0.086 in Ref. [22], which, however, is still far from the experimental value (-0.0048).

V. CONCLUSIONS

In this study the 3FD approach has been applied for the analysis of the recent STAR data on the directed flow of identified hadrons [20] together with earlier experimental data obtained at the SPS [17] and AGS [13]. Simulations have been done with a purely hadronic EoS [29] and two versions of the EoS involving deconfinement transitions [30]—a first-order phase transition and a smooth crossover transition—in the range of incident energies $\sqrt{s_{NN}} = 2.7-27$ GeV. Because of stringent requirements on the accuracy of the calculations we failed to perform calculations for energies above $\sqrt{s_{NN}} = 30$ GeV. The physical input of the present 3FD calculations is described in detail in Ref. [28]. No tuning (or change) of physical 3FD-model parameters and used EoS's has been done in the present study as compared to that stated in Ref. [28].

It was found that the proton directed flow within the deconfinement scenarios indeed manifests an antiflow (i.e., a negative slope of the v_1 distribution at the midrapidity), as predicted in Refs. [14,15]. This antiflow is tiny for the crossover EoS, which is in agreement with the data, and quite substantial for the EoS with the first-order phase transition. In the hadronic scenario, the midrapidity slope is always positive, except for the highest considered energy of $\sqrt{s_{NN}} = 27$ GeV, at which a tiny antiflow is observed. Note that the negative slope at midrapidity does not necessarily assume a QGP EoS. A combination of space-momentum correlations may result in a negative midrapidity slope of the directed flow in high-energy nucleus-nucleus collisions [18].

The excitation function of the slope of the v_1 distribution at the midrapidity for protons turns out to be a smooth function of the bombarding energy without "wiggle-like" peculiarities within the hadronic and crossover scenarios. At the same time, within the first-order-transition scenario this excitation function exhibits a wiggle predicted in Refs. [10,11,15,16]. In the present case the wiggle is mostly located in the negative range of slopes. The first-order-transition results demonstrate the worst agreement with the proton and antiproton data on the directed flow.

A high sensitivity of the directed flow, especially the proton one, to the nuclear EoS is found. Comparison of other bulk observables, analyzed so far [28,31–36], with available data indicated a definite advantage of the deconfinement (crossover and first-order) scenarios over the purely hadronic one, especially at high (RHIC) collision energies. However, predictions of the crossover and first-order-transition scenarios looked very similar so far. Only a slight preference could be given to the crossover EoS. In the case of the directed flow we can definitely conclude that the best overall reproduction of the STAR data is achieved with the crossover EoS. The first-order-transition scenario gives results which strongly differ from those in the crossover scenario, especially for the proton v_1.

The crossover scenario well reproduces the pion v_1 at all measured energies and the antiproton flow at $\sqrt{s_{NN}} > 10$ GeV.

Note that the 3FD model is poorly applicable to description of antiprotons at $\sqrt{s_{NN}} < 10$ GeV in view of a low antiproton multiplicity. In the case of proton slopes the crossover scenario fails both at low ($\sqrt{s_{NN}} < 5$ GeV) and high ($\sqrt{s_{NN}} > 20$ GeV) collision energies. The failure at low energies is still questionable because the same data but in terms of $\langle P_x \rangle$ are almost perfectly reproduced by the crossover scenario. As for the highest computed energy of $\sqrt{s_{NN}} = 27$ GeV, this simulation has been performed at the edge of computational abilities of the code. Therefore, the disagreement with the data could be, at least partially, because the 27-GeV results still suffer from insufficient accuracy. On the other hand, this disagreement may indicate a problem in the QGP sector of the used crossover EoS.

The the QGP sector of the EoS's with deconfinement [30] was fitted to the lattice QCD data at zero net-baryon density and just extrapolated to nonzero baryon densities. The comparison with v_1 data indicates that this QGP EoS at finite baryon densities is too soft, while the same EoS at zero net-baryon density, fitted to the lattice QCD data, is quite appropriate. Indeed, within the 3FD model the baryon-free (fireball) fluid is governed by the EoS at zero net-baryon density. This fluid is a main source of antiprotons, the directed flow of which is in good agreement with the data at $\sqrt{s_{NN}} = 27$ GeV within the crossover scenario, and in a reasonable agreement even within the first-order-transition scenario. The protons mainly originate from baryon-rich fluids which are governed by the EoS at finite baryon densities. The too-strong antiflow at $\sqrt{s_{NN}} = 27$ GeV within the crossover scenario is a sign of too-soft QGP EoS. Predictions of the first-order-transition EoS fail even at lower collision energies, i.e., right above the wiggle in the excitation function of the proton v_1 slope, when the QGP starts to dominate in the collision dynamics. This fact indirectly supports the conjecture on a too-soft QGP sector at high baryon densities in the used EoS's. The pions are produced from all (baryon-rich and baryon-free) fluids. Hence, the disagreement of the pion v_1 with data is quite moderate at $\sqrt{s_{NN}} = 27$ GeV.

Here it is appropriate to mention a discussion on the QGP EoS in astrophysics. In Ref. [53] it was demonstrated that the QGP EoS can be almost indistinguishable from the hadronic EoS at high baryon densities relevant to neutron stars. In particular, this gives a possibility of explaining hybrid stars with masses up to about 2 solar masses ($M_\odot$), in such a way that "hybrid stars masquerade as neutron stars" [53]. The discussion of such a possibility has been revived after measurements on two binary pulsars PSR J1614-2230 [54] and PSR J0348+0432 [55] resulted in the pulsar masses of $(1.97 \pm 0.04)M_\odot$ and $(2.01 \pm 0.04)M_\odot$, respectively. QCD motivated models show that such a "masquerade" is possible [56]: If the repulsive vector interaction is strong enough, it easily makes the QGP EoS sufficiently hard. In other words, to explain the existence of the neutron star with $\sim 2M_\odot$, a substantially large vector interaction should be expected. Probably, the results on the proton directed flow give us another indication of a required hardening of the QGP EoS at high baryon densities.

ACKNOWLEDGMENTS

Fruitful discussions with W. Cassing, V. P. Konchakovski, V. D. Toneev, and D. N. Voskresensky are gratefully acknowledged. We are grateful to A. S. Khvorostukhin, V. V. Skokov, and V. D. Toneev for providing us with the tabulated first-order-phase-transition and crossover EoS's. The calculations were performed at the computer cluster of GSI (Darmstadt). This work was partially supported by the Russian Ministry of Science and Education Grant No. NS-932.2014.2.

[1] P. Danielewicz and G. Odyniec, Phys. Lett. B **157**, 146 (1985).
[2] S. Voloshin and Y. Zhang, Z. Phys. C **70**, 665 (1996).
[3] S. A. Voloshin, A. M. Poskanzer, and R. Snellings, in *Relativistic Heavy Ion Physics*, Landolt-Boernstein New Series, I/23, edited by R. Stock (Springer Verlag, New York, 2010).
[4] H. Sorge, Phys. Rev. Lett. **78**, 2309 (1997).
[5] N. Herrmann, J. P. Wessels, and T. Wienold, Ann. Rev. Nucl. Part. Sci. **49**, 581 (1999).
[6] P. Danielewicz, R. Lacey, and W. G. Lynch, Science **298**, 1592 (2002).
[7] V. N. Russkikh and Yu. B. Ivanov, Phys. Rev. C **74**, 034904 (2006).
[8] L. P. Csernai and H. Stoecker, J. Phys. G **41**, 124001 (2014).
[9] C. M. Hung and E. V. Shuryak, Phys. Rev. Lett. **75**, 4003 (1995).
[10] D. H. Rischke, Y. Pursun, J. A. Maruhn, H. Stöcker, and W. Greiner, Heavy Ion Phys. **1**, 309 (1995).
[11] D. H. Rischke, Nucl. Phys. A **610**, 88 (1996).
[12] J. Barrette *et al.* (E877 Collaboration), Phys. Rev. C **56**, 3254 (1997).
[13] H. Liu *et al.* (E895 Collaboration), Phys. Rev. Lett. **84**, 5488 (2000).
[14] L. P. Csernai and D. Rohrich, Phys. Lett. B **458**, 454 (1999).
[15] J. Brachmann, S. Soff, A. Dumitru, H. Stöcker, J. A. Maruhn, W. Greiner, L. V. Bravina, and D. H. Rischke, Phys. Rev. C **61**, 024909 (2000).
[16] H. Stöcker, Nucl. Phys. A **750**, 121 (2005).
[17] C. Alt *et al.* (NA49 Collaboration), Phys. Rev. C **68**, 034903 (2003).
[18] R. J. M. Snellings, H. Sorge, S. A. Voloshin, F. Q. Wang, and N. Xu, Phys. Rev. Lett. **84**, 2803 (2000).
[19] M. M. Aggarwal *et al.* (STAR Collaboration), arXiv:1007.2613 [nucl-ex].
[20] L. Adamczyk *et al.* (STAR Collaboration), Phys. Rev. Lett. **112**, 162301 (2014).
[21] J. Steinheimer, J. Auvinen, H. Petersen, M. Bleicher, and H. Stöcker, Phys. Rev. C **89**, 054913 (2014).
[22] V. P. Konchakovski, W. Cassing, Yu. B. Ivanov, and V. D. Toneev, Phys. Rev. C **90**, 014903 (2014).
[23] H. Petersen, J. Steinheimer, G. Burau, M. Bleicher, and H. Stocker, Phys. Rev. C **78**, 044901 (2008).
[24] S. Bass *et al.*, Prog. Part. Nucl. Phys. **41**, 225 (1998).
[25] W. Cassing and E. L. Bratkovskaya, Nucl. Phys. A **831**, 215 (2009); Phys. Rev. C **78**, 034919 (2008); W. Cassing, Nucl. Phys. A **791**, 365 (2007).

[26] W. Cassing and E. L. Bratkovskaya, Phys. Rep. **308**, 65 (1999).
[27] Yu. B. Ivanov, V. N. Russkikh, and V. D. Toneev, Phys. Rev. C **73**, 044904 (2006).
[28] Yu. B. Ivanov, Phys. Rev. C **87**, 064904 (2013).
[29] V. M. Galitsky and I. N. Mishustin, Sov. J. Nucl. Phys. **29**, 181 (1979).
[30] A. S. Khvorostukhin, V. V. Skokov, K. Redlich, and V. D. Toneev, Eur. Phys. J. C **48**, 531 (2006).
[31] Yu. B. Ivanov, Phys. Rev. C **87**, 064905 (2013).
[32] Yu. B. Ivanov, Phys. Rev. C **89**, 024903 (2014).
[33] Yu. B. Ivanov, Phys. Lett. B **721**, 123 (2013).
[34] Yu. B. Ivanov, Phys. Lett. B **726**, 422 (2013).
[35] Yu. B. Ivanov, Phys. Lett. B **723**, 475 (2013).
[36] Yu. B. Ivanov, Phys. Rev. C **91**, 024914 (2015).
[37] I. N. Mishustin, V. N. Russkikh, and L. M. Satarov, Yad. Fiz. **48**, 711 (1988) [Sov. J. Nucl. Phys. **48**, 454 (1988)].
[38] V. N. Russkikh, Yu. B. Ivanov, Yu. E. Pokrovsky, and P. A. Henning, Nucl. Phys. A **572**, 749 (1994).
[39] I. N. Mishustin, V. N. Russkikh, and L. M. Satarov, Yad. Fiz. **54**, 429 (1991) [Sov. J. Nucl. Phys. **54**, 260 (1991)].
[40] U. Katscher, D. H. Rischke, J. A. Maruhn, W. Greiner, I. N. Mishustin, and L. M. Satarov, Z. Phys. A **346**, 209 (1993).
[41] J. Brachmann, A. Dumitru, J. A. Maruhn, H. Stöcker, W. Greiner, and D. H. Rischke, Nucl. Phys. A **619**, 391 (1997).
[42] Yu. B. Ivanov, Yad. Fiz. **46**, 100 (1987) [Sov. J. Nucl. Phys. **46**, 63 (1987)].
[43] Yu. B. Ivanov, Nucl. Phys. A **474**, 669 (1987).
[44] L. M. Satarov, Yad. Fiz. **52**, 412 (1990) [Sov. J. Nucl. Phys. **52**, 264 (1990)].
[45] Z. Xu and C. Greiner, Phys. Rev. C **71**, 064901 (2005).
[46] V. K. Magas, L. P. Csernai, and D. D. Strottman, Phys. Rev. C **64**, 014901 (2001).
[47] V. K. Magas, L. P. Csernai, and D. Strottman, Nucl. Phys. A **712**, 167 (2002).
[48] R. Waldhauser, D. H. Rischke, U. Katscher, J. A. Maruhn, H. Stoecker, and W. Greiner, Z. Phys. C **54**, 459 (1992).
[49] H. Appelshauser *et al.* (NA49 Collaboration), Phys. Rev. Lett. **80**, 4136 (1998).
[50] S. A. Bass, R. Mattiello, H. Stöcker, W. Greiner, and C. Hartnack, Phys. Lett. B **302**, 381 (1993).
[51] Yu. B. Ivanov and V. N. Russkikh, Phys. Rev. C **78**, 064902 (2008).
[52] B. B. Back, R. R. Betts, J. Chang, W. C. Chang, C. Y. Chi, Y. Y. Chu, J. B. Cumming, J. C. Dunlop *et al.*, Phys. Rev. C **66**, 054901 (2002).
[53] M. Alford, M. Braby, M. W. Paris, and S. Reddy, Astrophys. J. **629**, 969 (2005).
[54] P. Demorest, T. Pennucci, S. Ransom, M. Roberts, and J. Hessels, Nature (London) **467**, 1081 (2010).
[55] J. Antoniadis, P. C. C. Freire, N. Wex, T. M. Tauris, R. S. Lynch, M. H. van Kerkwijk, M. Kramer, C. Bassa *et al.*, Science **340**, 6131 (2013).
[56] K. Fukushima and C. Sasaki, Prog. Part. Nucl. Phys. **72**, 99 (2013).